Scottish Universities Environmental Research Centre

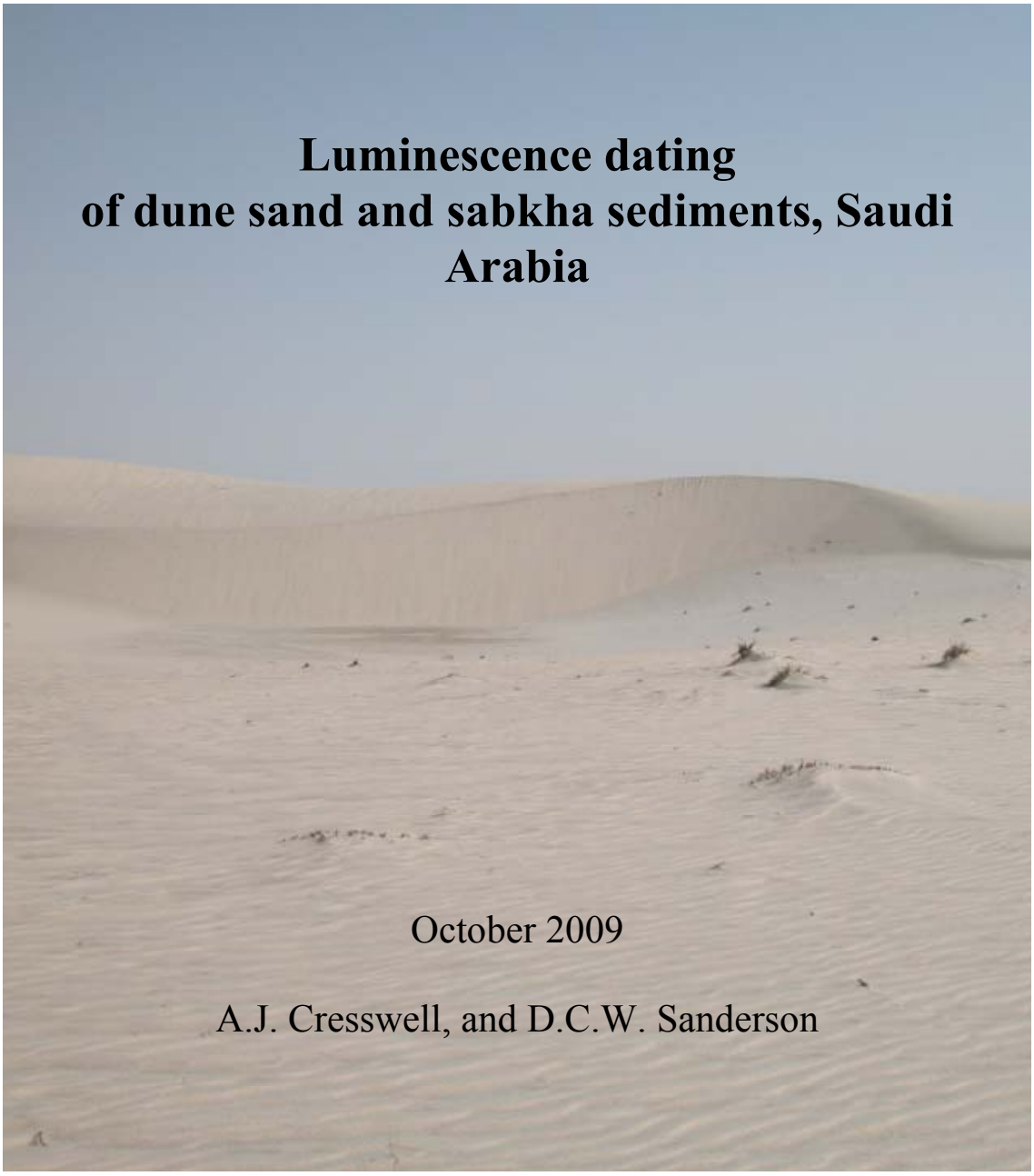

Luminescence dating of dune sand and sabkha sediments, Saudi Arabia

October 2009

A.J. Cresswell, and D.C.W. Sanderson

East Kilbride Glasgow G75 0QF Telephone: 01355 223332 Fax: 01355 229898

Summary

32 sediment samples recovered in April 2008 from active and relict dunes, and sabkhas/playas, in Saudi Arabia, were investigated using Optically Stimulated Luminescence (OSL) methods. This work follows an earlier investigation of similar sites over a larger area. The results of the current investigations are reported here.

The sabkha and shoreline samples show ages ranging from very modern (with no measurable OSL signal) to 7.6ka, indicating that this study area appears to have some sabkhas significantly younger than those observed in the earlier work.

One petrified dune sampled in this work produced an OSL date of 830±210 years, which is consistent with the age ranges of the petrified dunes sampled in the earlier work. Another showed very modern (with no measurable OSL signal) for the indurated sand at the top and an age of 200±150 years for the sand at the back of the dune; another sample taken nearby had an OSL age of 720±180 years. This dune appears to be much younger than the petrified dunes sampled in the previous study.

Samples from low-rolling dunes in this study have ages between very modern and 580 years. A barchan dune sample had an age of 60±30 years, similar to ages for barchan dunes sampled in the earlier work. Samples from a low hill had ages of 2.5±0.3 and 5.7±0.5 ka. A buried dune was sampled, producing no measurable natural OSL signal.

Contents

List of Figures

List of Tables

1. Introduction

This report is concerned with optically-stimulated luminescence (OSL) investigations of sediment samples recovered from active and relict dunes, and sabkhas/playas, in Saudi Arabia, c. 26°N 49°E to c. 25°N 50°E. Samples were taken by the client in April 2008. This work follows OSL investigations of 36 samples collected in the summer of 2006 from a larger area of Saudi Arabia (Burbidge et al 2007).

2. Sampling

Sampling was undertaken in April 2008 by the client, Stephen Franks. Samples were taken from the locations shown in Figure 2.1. Figure 2.2 shows these sampling sites along with the sites from the earlier work (Burbidge et al 2007). Sampling details, including the names assigned to each tube and bulk sample in the field, and the laboratory (SUTL) numbers assigned to each upon arrival at the SUERC luminescence dating laboratories, are summarised in Table 2.1. Photographs of the sampling sites are shown in Appendix A.

Figure 2.1. Map showing sampling locations for this work, with SUTL numbers

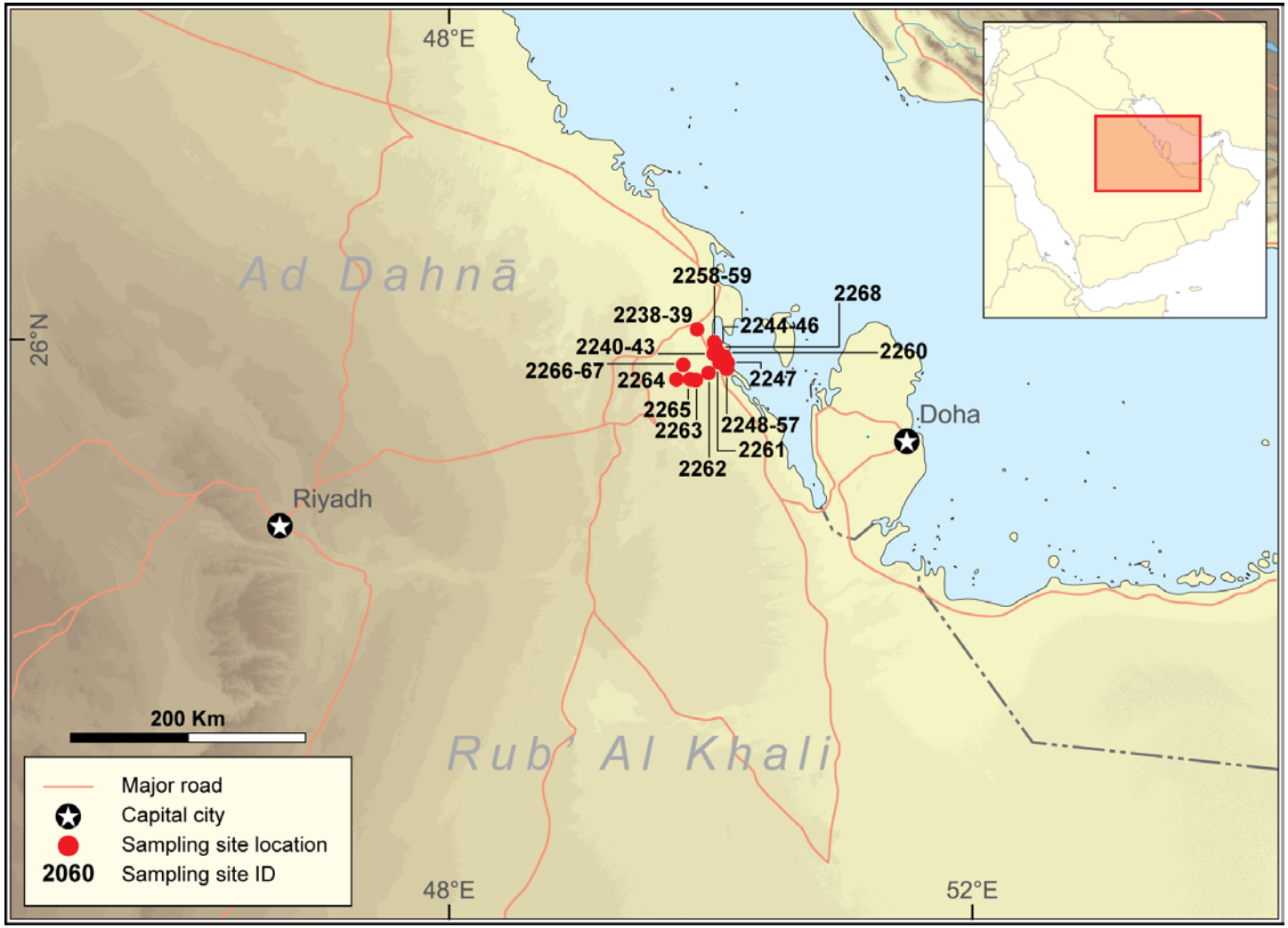

Figure 2.2. Map showing the sampling locations, with SUTL numbers, for this and the previous work

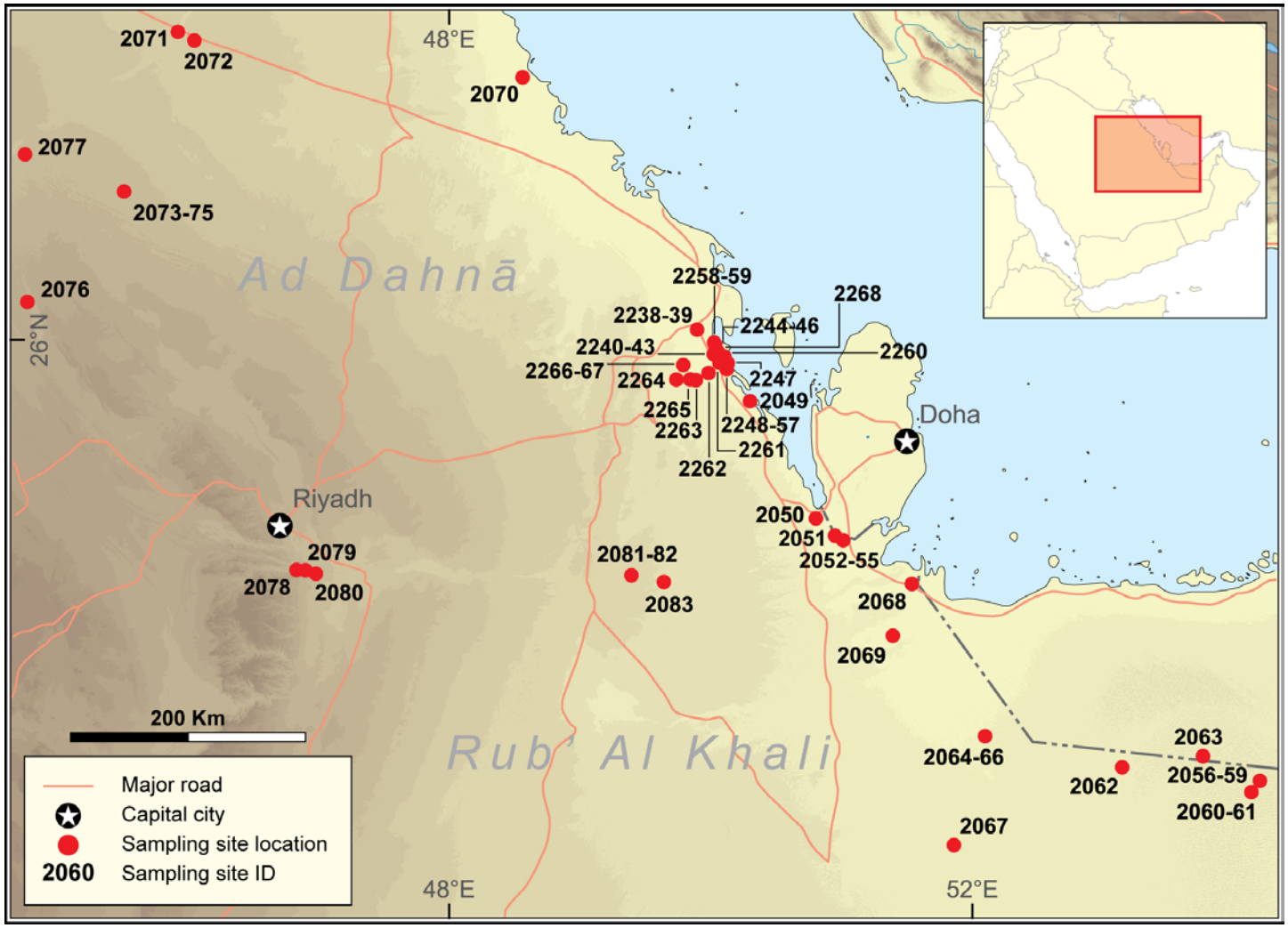

Table 2.1. Sample locations, descriptions, and SUERC laboratory numbers

Sample Number		Site		Sample Description	Depth (cm)
SUERC	Field	Coordinates	Description		
SUTL2237	OSL-21	26°04.141N 49°53.098E	Excavation in area of low rolling dunes 0 - 1.0 m cross-bedded dune sand with bioturbated top, dip 18° towards 144° 1.0 - 3.5 m cross-bedded dune sand, dip 14° towards 120-175° (estimated) 3.5 - 7.5 m low-angle tangential cross-bedded dune sand	Cross-bedded sand just below bioturbation surface	9
SUTL2238	OSL-22			From the youngest sand at top of the cross-bed, 7m SE from OSL-23	100
SUTL2239	OSL-23			Low-angle tangential cross-bedded sand, 20cm above base bed	730
SUTL2240	OSL-24	25°52.774N 50°01.165E	Sample from earlier trip near OSL 25 and OSL 26.		
SUTL2241	OSL-25	25°52.684N 50°01.385E	Petrified dune. Several tangentially cross-bedded sets with circa 2 m set height Large cross-beds near back, 27° dip towards 145° SE and 37° dip towards 230° SW (measured at top of cross-bed). Cross-bed at the front has 35° dip towards 197° S. The sediment surface is loose to crusty	From 80cm above base at the back of the petrified dune, white sand	120
SUTL2242	OSL-26			Indurated sand from the top of dune near the front, horizontal distance between OSL 25 and OSL 26 is 10 m	30
SUTL2243	OSL-28	25°53.005N 50°00.639E	Shallow trench on top of the back of barchan dune, high-angle foresets dipping 19° towards 155°S, white sand in white dune.		18
SUTL2244	OSL-29	25°57.468N 49°59.658E	Back of sabkha. Tangential foresets; upper laminae dipping 35° towards 215° S, flatter inclination of lower laminae. Anhydrite/gypsum crust on sand surface	From pit ~ 2 m above sabkha surface	200
SUTL2245	OSL-30	25°57.328N 50°01.333E	Sabkha. Thick light brown undulating crust, medium sand with some very fine grains, top 15cm sandier. cm-thick crinkly alternations of white and brown sand. Crystalline gypsum layer at 35cm. Brown sand with whitish layers near top		76
SUTL2246	OSL-31			Just above base of white sand	10
SUTL2247	OSL-36	25°48.845N 50°07.098E	Old shoreline. Trench dug on the eastern slope found crudely layered sand, thick white sand layer at top has orientation of 0.5° landward – W		9
SUTL2248	OSL-37	25°46.145N 50°09.551E	Sabkha. Cross-bedded dune sands, consisting of an alternation of light and dark laminae with a dip of 32° towards 195 ± 10° S, 10cm of sabkha sediment overlay	Dune foreset	29
SUTL2249	OSL-38			Sabkha sediments, depth ranges from 2.5 to 7.5 cm	5
SUTL2250	OSL-40	25°46.685N 50°08.075E	0 - 8 cm sabkha 8 - 21cm ripple sand 21 - 33 cm low-angle laminated sand, dip 10° towards S 33 - 49 cm slumped sand 49 - 89 cm high-angle cross-bedded sand, dip 30° towards S	From high-angle sand	73
SUTL2251	OSL-41			From slumped sand	50
SUTL2252	OSL-42			From low angle sand	30
SUTL2253	OSL-43			From rippled sand	20
SUTL2254	OSL-44	25°46.410N 50°06.681E	0 - 13 cm sabkha, ripple bed at base. Coarse, light coloured sand 13 - 23 cm sabkha, finely laminated darker sand 23 - 32 cm gypsum sand 32 - 76 cm sabkha	Upper sabkha (just above base)	14
SUTL2255	OSL-46			Lower sabkha	39
SUTL2256	OSL-47	25°46.092N 50°05.450E	Sediment with fairly regular lamination. A lower interval with more locally strong soft sediment deformation, and an upper interval. The boundary at 19 cm is irregular and gradual	From strong soft sediment deformation	55
SUTL2257	OSL-48			From sabkha with fairly regular lamination	15

SUTL2258	OSL-49	25°58.248N 50°00.925E	Slope of low hill 0 - 76 cm crudely bedded sand overlain by small-scale trough 76 - 103 cm sand bed with small scale trough cross-bedding 103 - 237 cm large scale cross-bedding dipping towards 140° SE		34
SUTL2259	OSL-51				149
SUTL2260	OSL-53	25°51.863N 50°05.586E	Low rolling dunes of circa 10 m thickness developed on bed rock. 0 - 50 cm sand covering base of exposure above bed rock 50 - 102 cm moderately rooted sand, subhorizontal lamination 102 - 124 cm weakly rooted sand, subhorizontal lamination and small scale cross-bedding 124 - 145 cm low-angle laminated sand 145 - 1000 cm apparently single dune foreset	Moderately rooted sand with subhorizontal lamination at 50cm above bed rock	950
SUTL2261	OSL-55	25°48.967N 50°03.353E	Excavation next to new road 0 - 48 cm horizontally laminated sand, bioturbated sand overlay 48 - 71 cm several sets of low-angle laminated sand, separated by thin horizontally laminated sand beds	From upper low-angle laminated sand bed at top of exposure	15
SUTL2262	OSL-59	25°44.326N 49°58.365E	Small sabkha in area of low rolling dunes. Sabkha surface is little crunchy, down-wind of small barchan dune. Distinct boundary at 20 cm depth separating thinly horizontally laminated sand and thicker laminated sand, showing some disturbance, below.		40
SUTL2263	OSL-61	25°41.104N 49°52.537E	Large sabkha with thick halite surface crust 0 - 21 cm darker sand 21 - 29 cm lighter sand 29 - 31 cm gypsum layer 31 - 43 cm indurated layer	From lighter sand	33
SUTL2264	OSL-64	25°41.360N 49°43.647E	Large sabkha near Hofuf river 0 - 10 cm dark sand with black lens 10 - 25 cm gypsiferous sand 25 - 78 cm slightly wavy sand	From slightly wavy sand	53
SUTL2265	OSL-64	25°41.419N 49°49.964E	Small sabkha (may have been dug) in area of low rolling dunes. 0 - 7 cm horizontally laminated crinkly light brown sand 7 - 14 cm sand with grey to dark brown and light brown colours 14 - 40 cm sand with black fill	Horizontally laminated crinkly light brown sand	10
SUTL2266	OSL-77	25°48.012N 49°46.793E	Sand within truncated top of buried dune foresets overlain by curvilinear berm-like topographic ridge with low-angle, bi-directional dips.	Steeply dipping, clean, crossbedded sand. Buried aeolian dune.	40
SUTL2267	OSL-78			Clean quartzose sandstone forming a low topographic berm with a broad crescentric shape (preserved lacustrine beach?).	20
SUTL2268	OSL-81	25°53.666N 50°02.826E	"Petrified" dunes; remnants of isolated, nebkha-like features with steep southerly dips.		

3. Methods

3.1. Sample preparation

All sample handling and preparation was conducted under safelight conditions in the SUERC luminescence dating laboratories.

Each horizontally sampled tube was subsampled for luminescence measurement (~10 g), dosimetry (>100 g), and water content determinations (~100 g). The boxed travel dosimeter was subsampled for luminescence measurement only.

Dosimetry subsamples were dried at 50 °C, and 100 g was weighed into HDPE pots for gamma spectrometry and 20 g was weighed into petri dishes for beta counting. The remainder was retained.

With the object of separating sand-sized quartz grains from the bulk sediment, luminescence subsamples were wet sieved to obtain 150-250 μm grains, which were treated with 1 M HCl for 10 minutes, to dissolve carbonates, and 40% Hydrofluoric acid (HF) for 40 minutes, to dissolve less chemically resistant minerals with a similar density to quartz, and to etch the outer part of the quartz grains, which would have absorbed external alpha radiation during burial. The HF etched material was then treated with 1 M HCl for 10 minutes to dissolve any precipitated fluorides. This etched quartz material was dried at 50°C, and dispensed in ~5 mg aliquots onto the central part of 1 cm diameter, 0.25 mm thick stainless steel disks, using silicone oil for adhesion. 16 disks were made per sample.

3.2. Measurements and determinations

3.2.1. Dose rate measurements and determinations

Dose rates were measured using Thick Source Beta Counting (TSBC) and High Resolution Gamma Spectrometry (HRGS). 20g of material was used for TSBC. For HRGS, 100g of material was sealed into HDPE pots (63mm internal diameter, 55mm depth) using epoxy resin and stored, to allow the daughters of any radon escaping from the samples to come into equilibrium, before measurement.

HRGS measurements were performed using a 50% relative efficiency “n” type hyperpure Ge detector (EG&G Ortec Gamma-X) operated in a low background lead shield with a copper liner. Gamma ray spectra were recorded over the 30 keV to 3 MeV range from each sample, interleaved with background measurements and measurements from Shap Granite in the same geometry. Counting times of between 25 and 80 ks per sample were used. The spectra were analysed to determine count rates from the major line emissions from ^{40}K (1461 keV), and from selected nuclides in the U decay series (^{234}Th, ^{226}Ra + ^{235}U, ^{214}Pb, ^{214}Bi and ^{210}Pb) and the Th decay series (^{228}Ac, ^{212}Pb, ^{208}Tl) and their statistical counting uncertainties. Net rates and activity concentrations for each of these nuclides were determined relative to Shap Granite by weighted combination of the individual lines for each nuclide. The internal consistency of nuclide specific estimates for U and Th decay series nuclides was assessed relative to measurement precision, and weighted combinations used to

estimate mean activity concentrations (in Bq kg^{-1}) and elemental concentrations (% K and ppm U, Th) for the parent activity. These data were used to determine infinite matrix dose rates for alpha, beta and gamma radiation.

Beta dose rates were also measured directly using the SUERC TSBC system (Sanderson, 1988). Sample count rates were determined with six replicate 600 s counts for each sample, bracketed by background measurements and sensitivity determinations using the SUERC Shap Granite secondary reference material. Infinite-matrix dose rates were calculated by scaling the net count rates of samples and reference material to the working beta dose rate of the Shap Granite (6.25±0.03 mGy a^{-1}). The estimated errors combine counting statistics, observed variance and the uncertainty on the reference value.

Water content measurements were conducted on bulk material extracted from the sample tubes into 100 ml beakers. The samples were weighed at the time of extraction (field water content). Water was added until it was observed that the structure of the core broke down, and the samples weighed to obtain the saturated mass. They were then dried at 50°C and reweighed. After subtracting the mass of the beaker, "field", and "saturated" values of water content were calculated as fractions of dry sediment mass. Note that to maintain bulk density, water content measurements are ideally made on material retained in the sampling tubes. However, given the size of these sampling tubes and the already loose sandy nature of most of the samples, the methodology outlined above was both more practicable and expected to yield sufficiently reliable results.

The dose rate estimates were used in combination with the measured water contents, to determine the overall effective dose rates for age estimation.

The cosmic dose rate is conventionally calculated rather than measured, without adjustment for sediment water content. The latitude, altitude and (sediment) depth dependencies of cosmic radiation, relevant to luminescence dating, are described by Prescott and Stephan (1982) and Prescott and Hutton (1988). In the present study, the latitude of each sample was approximated to the nearest degree, and altitude was approximated as 0.1 km for all. Surface cosmic dose rate was estimated using Prescott and Stephan (1982), Eqn. 1, with latitude dependent parameters read from Fig. 2. A representative value for the average burial depth of each sample since the luminescence signal was last zeroed, was estimated from depth at the time of sampling, geomorphological context, and approximate luminescence age. Depth was converted to mass-depth assuming sediment bulk density to be 1.6 g/cm^3, and a fit to the dose rate vs. depth data of Prescott and Hutton (1988) was used to calculate the cosmic dose rate at that depth. Uncertainties were calculated as: 5% plus the difference between cosmic dose rate at the depth of sampling, and that at the estimated average burial depth.

3.2.2. Luminescence measurements

All measurements were conducted using Risø DA-15 automatic readers, equipped with $^{90}Sr/^{90}Y$ β-sources for irradiation, blue LEDs emitting around 470 nm and infrared (laser) diodes emitting around 830 nm for optical stimulation, and a U340

detection filter pack to detect in the region 270-380 nm, while cutting out stimulating light (Bøtter-Jensen *et al*., 2000).

The discs of quartz grains from the tube samples were subjected to a single aliquot regeneration (SAR) sequence (Murray and Wintle, 2000). According to this procedure, the OSL signal level from an individual disc is calibrated to provide an absorbed dose estimate using an interpolated dose-response curve, constructed by regenerating OSL signals by irradiation in the laboratory. This estimate is termed the equivalent dose (De), since it is the laboratory dose producing an equivalent signal to that observed from the natural sample. Sensitivity changes which may occur as a result of readout, irradiation and preheating (to remove unstable radiation-induced signals) are monitored using small test doses after each regenerative dose. Each measurement is standardised to the test dose response determined immediately after its readout, thus compensating for observed changes in sensitivity during the laboratory measurement sequence.

In a SAR sequence then, each disc is subject to a number of measurement cycles: Natural&Test (cycle 1), Regenerative&Test (cycle 2), Regenerative&Test (cycle 3), etc., where all that is varied is the regenerative dose. For the purposes of interpolation, the regenerative doses are chosen to encompass the likely value of the equivalent (natural) dose. A repeat dose point is included to check the ability of the SAR procedure to correct for laboratory-induced sensitivity changes, a zero dose point is included late in the sequence to check for recuperative signals, and a repeat point with infrared stimulation prior to the OSL measurement is included to check for non-quartz signal ("Recycling", "Zero", "IRRecycling"; Table 4.1). Quartz responds to blue light but generally not to infrared light, whereas other common minerals such as feldspars and zircon respond to both. Additionally, results may vary with the severity of the preheating employed: this is tested for by applying a range of preheats to different groups within the set of discs.

In the present study 16 discs per sample were measured using 4 discs each at 4 different preheats (Table 3.1). Regenerative doses of 0 to 15 Gy were applied to all samples (plus repeats etc.: cycles 1 to 9, Table 3.1) and the results checked without removing the discs from the readers. If a sample yielded discs with equivalent doses exceeding 12 Gy, then additional regenerative points would have been added to put at least two above the majority of the equivalent dose values, and an extra recycling point was measured after these. In the samples measured here, no samples exceeded 12 Gy equivalent dose.

Table 3.1. Quartz Single Aliquot Regenerative Sequence

Aliquots	Operation	Cycle:	1	2	3	4	5	6	7	8	9
		Details	Natural	Linear-spaced low doses					Zero	Recycling	IR Recycling
1-16	Regenerative Dose	"X" Gy $^{90}Sr/^{90}Y$	no	3	6	9	12	15	0	3	3
1-4	Preheat	200°C for 30s	yes	yes	yes	yes	yes	yes	yes	yes	yes
4-8	Preheat	220°C for 30s	yes	yes	yes	yes	yes	yes	yes	yes	yes
9-12	Preheat	240°C for 30s	yes	yes	yes	yes	yes	yes	yes	yes	yes
13-16	Preheat	260°C for 30s	yes	yes	yes	yes	yes	yes	yes	yes	yes
1-16	Measurement	IRSL 120s at 50°C	no	no	no	no	no	no	no	no	yes
1-16	Measurement	OSL 60s at 125°C	yes	yes	yes	yes	yes	yes	yes	yes	yes
1-16	Test Dose	"X" Gy $^{90}Sr/^{90}Y$	1	1	1	1	1	1	1	1	1
1-16	Test Preheat	160°C for 30s	yes	yes	yes	yes	yes	yes	yes	yes	yes
1-16	Test Measurement	OSL 60s at 125°C	yes	yes	yes	yes	yes	yes	yes	yes	yes

4. Results

4.1. Dose rates

HGRS results are shown in Table 4.1, both as activity concentrations (i.e. disintegrations per second per kilogram) and as equivalent parent element concentrations (in % and ppm), based in the case of U and Th on combining nuclide specific data assuming decay series equilibrium. K concentrations ranged from 0.33 to 1.36 %, the mean was 0.77 ± 0.26%. U concentrations ranged from 0.10 to 1.09 ppm, the mean was 0.59 ± 0.24ppm. Th concentrations ranged from 0.57 to 2.68 ppm, the mean was 1.31 ± 0.50ppm. For comparison, “typical” values are 1 % K, 1 ppm U, and 3 ppm Th (Adamiec and Aitken, 1998).

The concentration ratio Th/U is also listed in Table 4.1, to indicate the relative contribution of Th and U to the samples’ dose rates. The “typical” context noted above has a concentration ratio of 3/1 (equivalent to an activity ratio of 1/1). Th/U for the present samples ranged from 1.45 to 6.30, with a mean value of 2.41 ± 0.93.

Infinite matrix alpha, beta and gamma dose rates from HGRS are listed in Table 4.2, with beta dose rates from TSBC, and the ratio of beta dose rates from TSBC/HGRS. Alpha dose rate (HGRS) ranged from 0.75 to 4.67 mGy/a, the mean was 2.60 ± 0.98 mGy/a. Gamma dose rate (HGRS) ranged from 0.13 to 0.49 mGy/a, the mean was 0.32 ± 0.09 mGy/a. Beta dose rate from HGRS ranged from 0.33 to 1.24 mGy/a, the mean was 0.76 ± 0.24 mGy/a. Beta dose rate from TSBC ranged from 0.35 to 1.33 mGy/a, the mean was 0.84 ± 0.25 mGy/a.

The mean ratio of beta dose rates from TSBC and HGRS was 1.12 ± 0.13, although the individual ratios were generally within 2σ of 1. The difference may result from differences in the radon retention conditions of each method. Whereas the HRGS measurements were conducted with sealed samples that had been stored for radon

equilibration, TSBC measurements were conducted in open geometry after drying the sample and would therefore not be expected to retain full equilibrium radon levels. To accommodate the range of likely sample conditions during burial, the average of the TSBC and HGRS values was used for the calculation of effective dose rates to the samples.

Effective dose rates to the HF etched 200 μm quartz grains used for equivalent dose determination in the present study are listed in Table 4.3, with water content measurements and the assumed values used for calculation of effective dose rate. Etching removes the external alpha contribution to the dose rate (so these are not tabulated). Cosmic dose rates are as calculated (section 3.2.1), gamma dose rates are corrected for water content, while beta dose rates are corrected for etching and water content.

Field water content, as a fraction of dry sediment mass, ranged from 0 to 0.18, the mean was 0.08 ± 0.06. Saturated water content ranged from 0.11 to 0.62, the mean was 0.27 ± 0.09. The field water contents were assumed to be low relative to the average the sample experienced during burial, such that the average value was most likely to lie between the measured field and saturated values. Assumed values for average water content during burial were estimated accordingly, and used for age determinations. These ranged from 0.05 to 0.34, the mean was 0.16 ± 0.06.

Effective beta dose rate ranged from 0.22 to 0.91 mGy/a, the mean was 0.61 ± 0.18 mGy/a. Effective gamma dose rate ranged from 0.10 to 0.40 mGy/a, the mean was 0.27 ± 0.08 mGy/a. Effective cosmic dose rate ranged from 0.13 to 0.27 mGy/a, the mean was 0.24 ± 0.04 mGy/a. On average, the beta contribution to overall dose rate was 55%, the gamma contribution was 24%, and the cosmic contribution was 21%.

Table 4.1. Activity and equivalent concentrations of K, U and Th, determined by HRGS

Sample SUTL	Activity Concentrations (Bq kg^{-1})			Equivalent Concentrations[1,2]			
	K	U	Th	K (%)	U (ppm)	Th (ppm)	Th/U
2237	122±7	6.9±0.3	4.1±0.3	0.39±0.02	0.55±0.02	1.01±0.07	1.84±0.14
2238	257±5	6.1±0.1	4.9±0.1	0.83±0.02	0.49±0.01	1.22±0.03	2.49±0.08
2239	206±8	7.4±0.3	4.1±0.3	0.67±0.03	0.60±0.02	1.02±0.07	1.70±0.13
2240	138±7	4.4±0.2	2.3±0.3	0.45±0.02	0.36±0.02	0.57±0.07	1.58±0.23
2241	117±6	4.6±0.3	3.2±0.3	0.38±0.02	0.37±0.02	0.80±0.08	2.16±0.25
2242	102±9	3.9±0.5	2.9±0.6	0.33±0.03	0.31±0.04	0.71±0.15	2.29±0.57
2243	231±7	7.3±0.2	4.7±0.2	0.75±0.02	0.59±0.02	1.17±0.05	1.98±0.11
2244	360±6	9.4±0.2	6.6±0.1	1.17±0.02	0.76±0.01	1.62±0.03	2.14±0.05
2245	347±10	7.3±0.3	7.5±0.3	1.12±0.03	0.59±0.02	1.86±0.07	3.14±0.16
2246	180±10	13.4±0.7	9.0±0.6	0.58±0.03	1.09±0.06	2.23±0.15	2.05±0.18
2247	213±11	6.3±0.5	4.5±0.5	0.69±0.03	0.51±0.04	1.11±0.13	2.16±0.30
2248	308±13	8.2±0.5	7.9±0.6	1.00±0.04	0.66±0.04	1.95±0.15	2.95±0.29
2249	219±8	12.0±0.4	5.7±0.3	0.71±0.03	0.97±0.03	1.41±0.08	1.46±0.09
2250	243±8	4.4±0.3	3.2±0.3	0.79±0.03	0.36±0.02	0.78±0.07	2.17±0.23
2251	179±8	4.9±0.3	4.5±0.3	0.58±0.03	0.39±0.02	1.10±0.07	2.80±0.23
2252	295±13	8.9±0.6	5.3±0.6	0.96±0.04	0.72±0.05	1.32±0.14	1.83±0.23
2253	156±6	4.7±0.2	3.4±0.2	0.51±0.02	0.38±0.01	0.84±0.04	2.21±0.12
2254	188±7	6.7±0.3	5.3±0.3	0.61±0.02	0.55±0.02	1.31±0.07	2.39±0.16
2255	162±11	11.7±0.7	6.8±0.6	0.52±0.04	0.95±0.05	1.67±0.15	1.76±0.18
2256	231±7	7.2±0.2	4.7±0.3	0.75±0.02	0.58±0.02	1.17±0.07	2.02±0.14
2257	222±11	9.8±0.6	6.0±0.6	0.72±0.04	0.79±0.05	1.48±0.14	1.87±0.21
2258	237±11	8.1±0.6	6.3±0.6	0.77±0.04	0.66±0.05	1.56±0.15	2.36±0.29
2259	210±11	7.1±0.5	4.7±0.6	0.68±0.03	0.57±0.04	1.16±0.14	2.02±0.28
2260	228±9	11.0±0.4	10.9±0.3	0.74±0.03	0.89±0.03	2.68±0.08	3.00±0.14
2261	281±5	11.8±0.2	7.5±0.1	0.91±0.02	0.96±0.01	1.84±0.02	1.92±0.03
2262	313±13	5.3±0.5	4.8±0.6	1.01±0.04	0.43±0.04	1.18±0.14	2.77±0.42
2263	288±12	4.5±0.5	3.2±0.5	0.93±0.04	0.37±0.04	0.78±0.13	2.13±0.42
2264	344±13	7.3±0.5	5.1±0.6	1.11±0.04	0.59±0.04	1.26±0.14	2.14±0.28
2265	363±10	11.7±0.4	7.7±0.3	1.17±0.03	0.95±0.03	1.90±0.08	2.00±0.11
2266	299±7	3.5±0.2	3.3±0.2	0.97±0.02	0.28±0.01	0.81±0.05	2.89±0.21
2267	422±10	4.9±0.3	7.4±0.3	1.36±0.03	0.39±0.02	1.82±0.08	4.67±0.32
2268	110±7	1.3±0.2	2.5±0.3	0.36±0.02	0.10±0.02	0.63±0.07	6.01±1.37

[1] Conversion factors (based on OECD, 1994):
^{40}K : 309.26 Bq kg-1 %K^{-1} ; ^{238}U : 12.34787 Bq kg^{-1} ppmU^{-1} ; ^{232}Th : 4.057174 Bq kg^{-1} ppmTh^{-1}.

[2] Working values for Shap Granite:
4.43±0.03%K, 12.00±0.06 ppm U, 28.5±0.26 ppm Th.
^{40}K: 1370±10 Bq kg^{-1}, ^{238}U: 148.17±7.4 Bq kg^{-1}, ^{232}Th: 115.6±1.05 Bq kg^{-1}.
Based on HRGS relative to CANMET and NBL standards (Sanderson, 1986).

Table 4.2. Infinite matrix dose rates determined by HRGS and TSBC

Sample SUTL	Dry Infinite Matrix dose rates[1] by HRGS (mGy a^{-1})			TSBC (mGy a^{-1})	TSBC/HRGS Beta ratio
	D_α (dry)	D_β (dry)	D_γ (dry)	D_β (dry)	
2237	2.28±0.08	0.44±0.02	0.211±0.007	0.352±0.037	0.80±0.09
2238	2.26±0.03	0.80±0.01	0.319±0.004	0.912±0.043	1.14±0.06
2239	2.42±0.09	0.67±0.02	0.281±0.008	0.879±0.043	1.31±0.08
2240	1.41±0.07	0.44±0.02	0.178±0.007	0.507±0.039	1.15±0.10
2241	1.62±0.08	0.39±0.02	0.174±0.007	0.376±0.027	0.96±0.08
2242	1.40±0.15	0.34±0.02	0.153±0.011	0.361±0.027	1.06±0.10
2243	2.50±0.06	0.74±0.02	0.308±0.006	1.007±0.044	1.36±0.07
2244	3.30±0.04	1.12±0.02	0.451±0.005	1.155±0.045	1.03±0.04
2245	3.01±0.09	1.07±0.03	0.434±0.009	1.087±0.045	1.02±0.05
2246	4.67±0.19	0.71±0.03	0.380±0.013	0.801±0.042	1.13±0.08
2247	2.24±0.15	0.68±0.03	0.282±0.012	0.764±0.041	1.12±0.08
2248	3.27±0.17	0.97±0.03	0.416±0.014	1.065±0.045	1.10±0.06
2249	3.75±0.11	0.77±0.02	0.355±0.008	0.779±0.042	1.01±0.06
2250	1.57±0.08	0.73±0.02	0.270±0.008	0.753±0.041	1.03±0.06
2251	1.91±0.08	0.57±0.02	0.242±0.008	0.771±0.042	1.35±0.09
2252	2.97±0.17	0.94±0.03	0.380±0.013	1.041±0.044	1.11±0.06
2253	1.67±0.05	0.50±0.02	0.209±0.005	0.613±0.040	1.23±0.09
2254	2.48±0.08	0.62±0.02	0.277±0.007	0.857±0.042	1.38±0.08
2255	3.87±0.19	0.62±0.03	0.321±0.013	0.718±0.041	1.16±0.09
2256	2.47±0.07	0.74±0.02	0.307±0.007	0.824±0.031	1.11±0.05
2257	3.29±0.17	0.75±0.03	0.340±0.012	0.933±0.043	1.24±0.08
2258	2.99±0.17	0.78±0.03	0.341±0.013	0.888±0.031	1.14±0.06
2259	2.44±0.16	0.68±0.03	0.288±0.012	0.715±0.041	1.05±0.08
2260	4.46±0.11	0.82±0.02	0.418±0.009	0.983±0.044	1.20±0.06
2261	4.02±0.04	0.95±0.01	0.423±0.004	0.914±0.043	0.96±0.05
2262	2.06±0.16	0.94±0.03	0.353±0.012	0.985±0.044	1.05±0.06
2263	1.60±0.15	0.85±0.03	0.307±0.013	0.862±0.042	1.01±0.06
2264	2.56±0.16	1.04±0.04	0.400±0.013	1.069±0.045	1.03±0.06
2265	4.05±0.11	1.17±0.03	0.490±0.010	1.325±0.047	1.13±0.05
2266	1.38±0.05	0.87±0.02	0.307±0.006	1.022±0.044	1.17±0.06
2267	2.44±0.08	1.24±0.03	0.468±0.009	1.221±0.046	0.98±0.04
2268	0.75±0.07	0.33±0.02	0.130±0.007	0.387±0.038	1.17±0.14

[1] Based on Dose Rate conversion factors from Aitken, 1983.

Table 4.3. Water contents and effective dose rates

Sample SUTL	Water Content			Effective dose rates (mGy a^{-1})			
	FW %	SW %	Assumed %	Beta[1]	Gamma[2]	Cosmic[3]	Total
2237	0.3	16.5	7.6±2.7	0.33±0.04	0.194±0.008	0.269±0.023	0.79±0.04
2238	1.8	21.1	10.4±2.9	0.69±0.04	0.286±0.009	0.208±0.033	1.19±0.05
2239	1.1	21.0	10.0±3.0	0.63±0.04	0.253±0.010	0.139±0.046	1.02±0.06
2240	8.1	35.3	19.9±3.4	0.35±0.03	0.146±0.007	0.268±0.026	0.76±0.04
2241	7.7	44.5	23.9±4.0	0.27±0.02	0.138±0.007	0.201±0.032	0.61±0.04
2242	12.7	62.3	34.4±4.7	0.22±0.03	0.111±0.009	0.248±0.033	0.58±0.04
2243	2.6	27.9	13.9±3.4	0.68±0.04	0.267±0.010	0.259±0.029	1.21±0.05
2244	1.8	31.4	15.0±3.6	0.89±0.05	0.391±0.014	0.185±0.031	1.47±0.06
2245	11.9	23.1	16.3±2.1	0.82±0.04	0.367±0.010	0.218±0.035	1.41±0.06
2246	5.7	24.9	14.0±2.9	0.58±0.04	0.329±0.014	0.268±0.024	1.17±0.05
2247	0.3	25.0	11.4±3.3	0.58±0.05	0.250±0.013	0.269±0.023	1.10±0.05
2248	11.4	23.2	16.2±2.2	0.78±0.05	0.353±0.014	0.249±0.034	1.38±0.06
2249	11.8	27.1	18.1±2.5	0.57±0.04	0.296±0.010	0.274±0.020	1.14±0.04
2250	14.3	19.7	16.0±1.3	0.57±0.04	0.230±0.007	0.219±0.035	1.02±0.05
2251	8.0	23.4	14.5±2.6	0.52±0.04	0.208±0.008	0.232±0.036	0.96±0.05
2252	8.7	26.5	16.3±2.8	0.74±0.05	0.322±0.014	0.248±0.034	1.31±0.06
2253	2.3	23.8	11.9±3.1	0.44±0.04	0.184±0.007	0.257±0.030	0.88±0.05
2254	3.2	25.4	13.0±3.1	0.58±0.04	0.242±0.010	0.263±0.027	1.09±0.05
2255	11.4	26.3	17.5±2.5	0.50±0.04	0.269±0.013	0.240±0.036	1.01±0.06
2256	18.5	26.1	21.0±1.6	0.57±0.03	0.249±0.006	0.229±0.036	1.04±0.05
2257	7.3	26.4	15.5±2.9	0.64±0.04	0.290±0.013	0.262±0.028	1.19±0.05
2258	1.5	11.0	5.7±2.0	0.72±0.05	0.320±0.014	0.244±0.035	1.29±0.06
2259	1.2	27.9	13.2±3.5	0.55±0.04	0.252±0.013	0.194±0.031	0.99±0.06
2260	3.0	23.2	12.0±3.0	0.71±0.05	0.369±0.013	0.125±0.047	1.20±0.07
2261	2.1	20.9	10.5±2.9	0.75±0.04	0.379±0.012	0.262±0.028	1.39±0.05
2262	16.4	25.5	19.7±1.8	0.71±0.04	0.290±0.012	0.239±0.036	1.24±0.06
2263	5.1	22.6	12.7±2.8	0.68±0.05	0.269±0.013	0.245±0.035	1.19±0.06
2264	18.1	24.8	20.2±1.5	0.78±0.04	0.327±0.012	0.230±0.036	1.33±0.06
2265	18.3	24.3	20.0±1.3	0.91±0.04	0.401±0.009	0.268±0.024	1.58±0.05
2266	10.6	28.5	18.1±2.7	0.71±0.04	0.256±0.008	0.239±0.036	1.21±0.06
2267	10.9	30.7	19.2±2.9	0.91±0.05	0.386±0.013	0.257±0.030	1.56±0.06
2268	11.0	47.0	26.7±4.0	0.25±0.03	0.100±0.006	0.268±0.026	0.62±0.04

[1] Calculated using the average of the infinite beta dose rates measured using HRGS and TSBC: effective beta dose rate = (1-φ)*infinite beta dose rate/(1+1.25*water content).
φ is the absorbed dose fraction in a 200 micron silicate grain weighted by the U, Th and K concentrations determined by HRGS (Mejdahl, 1979).

[2] Effective gamma dose rate = infinite gamma dose rate/(1+1.14*water content).
For the energies found in a typical sedimentary matrix, water absorbs approximately 1.25 times more beta, and 1.14 times more gamma radiation per unit mass than do silicates (Aitken, 1985).

[3] Calculated from latitude, altitude, and estimated average depth during burial, using the data of Prescott and Stephan (1982) and Prescott and Hutton (1988).

4.2. Single aliquot equivalent dose determinations

Sample averaged values relating to the aliquots and measurements used for equivalent dose determination are listed in Table 4.4.

The average sensitivity of the OSL signal from these samples to radiation ranged from 33 to 437 cps/Gy, the mean was 176 ± 108 cps/Gy. With repeated SAR measurement cycles, this sensitivity changed to between 0.26 and 1.9 times the starting values, the mean being 0.9 ± 0.3 times. With respect to the internal checks on SAR performance: average recycling ratio for each sample ranged between 0.95 and 1.93, with a mean of 1.14 ± 0.17, and the effect of IRSL exposure on this ratio was to produce a range of 0 to 29%, with a mean of 8 ± 8%.

For equivalent dose determination, data from single aliquot regenerative dose measurements were analysed using the Risø TL/OSL Viewer programme to export integrated summary files that were analysed in MS Excel and SigmaPlot. Dose response curves for each of the four pre-heating temperature groups and the combined data were determined using a fit to a saturating exponential function in the first instance. Where the exponential fit was poorly constrained a linear fit was used. Values of De were determined for each group of disks and each individual disk.

Arithmetic mean De values are listed for each sample in Table 4.4, with the estimated uncertainty on the mean value (standard deviation divided by the square root of the number of disks), and the standard deviation of the dataset. The mean De values range from –0.48 to 10.75 Gy, although the average is 1.5 ± 2.8 Gy. However, examination of the distributions of results from individual aliquots indicated that some of the mean values were affected by scatter in the data and some data with poor precision. Weighted means are given that reduce the influence of low precision data points. These range from –0.01 to 8.86Gy with an average of 1.2±2.3 Gy. Robust mean De data generated using Huber's estimate 2 (H15) using the Royal Society of Chemistry robust statistics toolkit for MS Excel (Ellison 2002). These range from –0.06 to 10.61 Gy with an average of 1.5±2.7 Gy.

The selection of an appropriate best estimate for De was made on a case by case basis, by examining plots of De for each disk in the data sets. The comment column in Table 4.4 indicates the basis of the decision in each case. In several cases, one of the means calculated was strongly influenced by either low precision data points or outliers. In instances where there was a clearly defined group of discs with the same De, especially where these had good precision, with some outliers the De for the grouping is given.

Sample SUTL2268 generated signals with very low sensitivity, resulting in very poor reproducibility in response to the test dose. The OSL measurements were repeated twice, yet only five discs from all three data sets produced data that could be used for estimating the age.

Table 4.4. Equivalent dose determination: samples and results

Sample SUTL	Risø	Mean Sensitivity (counts Gy^{-1})	Sensitivity change (%)	Recycling ratio	Post IRSL ratio (%)	Mean De Estimates (Gy)				Comment
						Linear	Weighted	Robust	Best estimate	
2237	2	195±25	68±37	1.13±0.15	7.0±0.4	0.32±0.05	0.24±0.05	0.33±0.05	0.32±0.05	
2238	2	198±25	83±39	1.13±0.14	7.5±0.5	0.44±0.08	0.31±0.05	0.43±0.08	0.31±0.05	7 discs at 0.3Gy, 7 discs at 0.6±0.2Gy
2239	2	194±27	108±48	1.12±0.13	5.7±0.4	-0.03±0.06	-0.01±0.02	-0.06±0.05		Below measurement limit
2240	2	47±6	127±40	1.11±0.32	-2.7±3.1	-0.48±0.68	0.56±0.14	-0.02±0.35	0.56±0.14	7 discs, 5 high precision, at 0.5±0.2Gy. 4 low precision discs <0Gy
2241	1	34±2	74±9	1.36±0.77	28.0±2.8	0.62±0.21	0.12±0.09	0.51±0.16	0.12±0.09	7 high precision discs at 0.15±0.10Gy. 7 lower precision discs at 0.6±0.2Gy
2242	2	33±2	76±14	1.93±1.68	4.2±4.1	0.49±0.17	-0.01±0.13	0.47±0.19		7 high precision discs at ~0Gy. 7 lower precision discs at 1±1Gy
2243	2	190±33	83±54	1.23±0.18	8.5±0.5	0.08±0.09	0.01±0.02	0.06±0.03	0.07±0.03	1 disc outlier at 1.1±0.6Gy. 1 disc at –0.7±0.8Gy
2244	2	137±14	103±34	1.21±0.19	9.9±0.7	0.21±0.12	0.09±0.05	0.16±0.08	0.16±0.08	10 discs at 0.2±0.1Gy. 2 discs at 1.2±1.0Gy. 4 discs <0Gy
2245	2	291±43	55±39	1.01±0.09	5.1±0.3	10.75±0.71	8.86±0.71	10.61±0.73	10.70±0.70	
2246	2	188±32	111±58	1.02±0.13	7.7±0.5	-0.03±0.06	0.05±0.02	0.01±0.04	0.05±0.02	4 low precision discs <0Gy
2247	2	328±54	26±37	1.09±0.10	4.0±0.3	6.95±0.80	6.17±0.12	6.26±0.33	6.26±0.33	1 high precision disc at 10.8±0.3Gy. 1 low precision disc at 17±19Gy
2248	1	43±11	119±87	1.18±0.31	14.0±6.0	-0.43±0.54	0.22±0.14	0.04±0.36	0.22±0.14	3 low precision discs at <0Gy
2249	2	170±40	123±85	1.12±0.18	5.5±0.5	0.01±0.09	0.05±0.03	-0.03±0.07		Below measurement limit. 1 low precision disc at 1±1Gy
2250	2	38±7	61±45	1.12±0.59	-2.9±9.3	1.64±0.29	0.09±0.21	1.64±0.41	1.64±0.29	1high precision disc at –0.2±0.2
2251	2	79±10	85±38	1.24±0.56	8.4±1.5	0.74±0.11	0.53±0.09	0.74±0.11	0.74±0.11	
2252	1	374±125	167±137	1.06±0.12	13.8±0.4	1.23±0.08	1.03±0.07	1.24±0.08	1.23±0.08	1 disc at 0.5±0.1Gy
2253	2	156±40	53±67	1.32±0.45	4.0±1.5	0.87±0.16	0.53±0.07	0.90±0.16	0.90±0.16	
2254	1	110±14	98±40	1.20±0.29	17.7±0.08	-0.08±0.07	0.04±0.02	-0.04±0.06	0.04±0.06	8 discs at 0.04Gy with good precision, 5 low precision discs <0Gy
2255	2	127±37	81±89	1.12±0.26	4.3±2.3	1.08±0.21	0.63±0.15	0.99±0.18	0.99±0.18	1 disc at 3.5±3.8Gy
2256	1	96±20	96±68	1.06±0.25	3.5±1.6	0.52±0.42	0.03±0.02	0.10±0.09	0.10±0.09	1 disc at 6±3Gy
2257	1	175±90	99±170	1.06±0.54	1.2±11.2	0.56±0.55	0.02±0.04	0.13±0.11		Below measurement limit. 13 high precision discs at 0Gy, 3 outliers at 8±6Gy, 3±1Gy and –3±3Gy
2258	1	267±46	68±49	1.02±0.11	7.5±0.4	7.39±0.49	6.08±0.58	7.39±0.56	7.39±0.49	Poor precision on all data (25-40%), limited scatter
2259	1	437±78	80±53	0.98±0.06	29.1±0.3	2.43±0.20	1.27±0.13	2.42±0.18	2.43±0.20	1 disc at 0.7±0.2Gy influencing weighted mean
2260	1	393±57	43±36	1.01±0.07	11.8±0.4	1.84±0.44	0.70±0.05	1.63±0.37	0.70±0.05	10 high precision discs at 0.7Gy, 6 low precision at 3-6Gy
2261	1	224±26	96±37	1.07±0.22	3.4±0.6	8.58±0.61	6.66±0.75	8.55±0.63	8.58±0.61	1 disc at 5Gy with high precision influencing weighted mean
2262	2	298±129	91±137	0.95±0.12	2.3±1.4	0.10±0.08	0.07±0.02	0.09±0.05	0.07±0.02	Some low precision outliers
2263	1	78±11	129±51	1.03±0.27	5.1±1.8	1.50±0.17	1.45±0.18	1.53±0.16	1.50±0.17	
2264	1	218±26	113±42	1.05±0.10	7.9±0.3	0.04±0.03	0.00±0.01	0.04±0.03		Below measurement limit
2265	1	149±15	84±29	1.12±0.13	20.6±1.0	0.99±0.12	0.83±0.08	0.93±0.10	0.83±0.08	Some lower precision discs at 1-2Gy
2266	2	180±26	91±45	1.12±0.15	8.0±0.4	-0.05±0.03	-0.01±0.02	-0.05±0.03		Below measurement limit
2267	1	93±5	111±15	1.15±0.21	20.1±1.5	0.05±0.07	0.01±0.03	0.02±0.05		Below measurement limit. 2 discs at 0.6±0.6Gy
2268	1	83±85	192±443	1.20±0.13	-1.8↓0.8	0.51±0.12	0.42±0.14	0.51±0.13	0.51±0.12	Only 5 discs in three runs should reproducible results

4.3. Age estimates

Listed in Table 4.5 are the sums of the effective beta, gamma and cosmic dose rates and the best estimate mean equivalent dose values. Age values were calculated as equivalent dose divided by dose rate, and converted to calendar dates.

Dose rate ranges from 0.58 to 1.58 mGy/a, the average is 1.12 ± 0.26mGy/a. De values range from 0.00 to 10.7 Gy, the average is 1.5 Gy ± 2.8. Age estimates for these samples range from 0.0 to 7.6 ka, with an average of 1.4 ± 2.2 ka. Percentage uncertainty is very high (>40%) for age estimates close to zero, for the remainder uncertainties are 7 - 25. The main source of age uncertainty at this level of precision lies with the OSL determination of equivalent dose. For well bleached samples it is possible that this could be improved to the limits of dose rate uncertainty (typically 5-10%) by utilising larger numbers of aliquots, or by using larger sized aliquots. The dose rate uncertainties themselves are limited by the uncertainty of past water content determination, and for the lowest dose rate samples (eg below 0.5 mGy/a) by the signal to background ratios of the beta and gamma spectrometry systems used.

Table 4.5. Dose rates, equivalent doses, ages and calendar dates

Sample		Total Dose Rate ($mGy\ a^{-1}$)	Equivalent Dose (Gy)	Age (ka)	% error	Calender Date
SUTL	Field					
2237	OSL-21	0.79±0.04	0.33±0.05	0.41±0.07	17	1600±70 AD
2238	OSL-22	1.19±0.05	0.31±0.05	0.26±0.04	15	1750±40 AD
2239	OSL-23	1.02±0.06	Below measurement limit			
2240	OSL-24	0.76±0.04	0.56±0.14	0.74±0.19	25	1275±190 AD
2241	OSL-25	0.61±0.04	0.12±0.09	0.20±0.15	75	1800±150 AD
2242	OSL-26	0.58±0.04	Below measurement limit			
2243	OSL-28	1.21±0.05	0.07±0.03	0.06±0.03	50	1950±25 AD
2244	OSL-29	1.47±0.06	0.16±0.08	0.11±0.05	50	1900±55 AD
2245	OSL-30	1.41±0.06	10.70±0.70	7.61±0.58	8	5600±580 BC
2246	OSL-31	1.17±0.05	0.05±0.02	0.04±0.02	50	1965±20 AD
2247	OSL-36	1.10±0.05	6.26±033	5.71±0.41	7	3700±410 BC
2248	OSL-37	1.38±0.06	0.22±0.14	0.16±0.10	63	1850±100 AD
2249	OSL-38	1.14±0.04	Below measurement limit			
2250	OSL-40	1.02±0.05	1.64±0.29	1.61±0.30	19	395±300 AD
2251	OSL-41	0.96±0.05	0.74±0.11	0.77±0.12	16	1240±120 AD
2252	OSL-42	1.31±0.06	1.23±0.08	0.94±0.07	7	1070±75 AD
2253	OSL-43	0.88±0.05	0.90±0.16	1.02±0.19	19	990±190 AD
2254	OSL-44	1.09±0.05	0.04±0.02	0.04±0.02	50	1970±20 AD
2255	OSL-46	1.01±0.06	0.99±0.18	0.98±0.19	19	1025±185 AD
2256	OSL-47	1.04±0.05	0.10±0.09	0.10±0.09	90	1915±85 AD
2257	OSL-48	1.19±0.05	Below measurement limit			
2258	OSL-49	1.29±0.06	7.39±0.49	5.74±0.47	8	3700±470 BC
2259	OSL-51	0.99±0.06	2.43±0.20	2.45±0.25	10	440±250 BC
2260	OSL-53	1.20±0.07	0.70±0.05	0.58±0.05	9	1425±55 AD
2261	OSL-55	1.39±0.05	8.58±0.61	6.17±0.50	8	4150±500 BC
2262	OSL-59	1.24±0.06	0.07±0.02	0.05±0.02	40	1955±20 AD
2263	OSL-61	1.19±0.06	1.50±0.17	1.25±0.15	12	750±150 AD
2264	OSL-64	1.33±0.06	Below measurement limit			
2265	OSL-64	1.58±0.05	0.83±0.08	0.53±0.05	9	1480±50 AD
2266	OSL-77	1.21±0.06	Below measurement limit			
2267	OSL-78	1.56±0.06	Below measurement limit			
2268	OSL-81	0.62±0.04	0.51±0.12	0.83±0.21	25	1180±200 AD

5. Discussion

A number of points noted in the Methods and Results sections merit further discussion (sections 3 and 4 respectively).

5.1. Dosimetry

Radionuclide concentrations in general were lower than is commonly observed, reflecting the low activity nature of the quartz rich Aeolian sands that form the basis for most of the sediments in the present study. They do not appear to relate strongly to geographical location, and probably depend more strongly on a sample's source material and depositional context. U and Th readily adsorb onto clays, so U and Th activity is likely to broadly correlate with clay content.

5.2. Equivalent dose determination

Of the 32 samples processed, 7 samples (SUTL2239, 2242, 2249, 2257, 2264, 2266 and 2267) had no measurable natural signal and correspond to modern samples. 7 samples (SUTL2241, 2243, 2244, 2246, 2254, 2256, 2262) had an equivalent dose less than 0.2Gy, with >50% uncertainty. A further 3 samples (SUTL2237, 2238, 2248) had equivalent doses between 0.2 and 0.5Gy, with 15-50% uncertainty. 7 samples (SUTL2240, 2251, 2253, 2255, 2260 and 2268) had equivalent doses of between 0.5 and 1.0Gy, and 8 samples (SUTL2245, 2247, 2250, 2252, 2258, 2259, 2261 and 2263) had equivalent doses greater than 1Gy.

In the earlier work (Burbidge et al 2007), a similar proportion of the samples had low equivalent doses (below 0.2Gy) as in the current work. In that work, a much larger proportion of the samples had equivalent doses above 1Gy, with 9 samples in the earlier work with equivalent doses greater than the maximum observed in this work.

5.3. Ages

Grouping the samples in geographical locations:

1/ Low rolling dunes (SUTL2237-2239; OSL-21, OSL-22, OSL-23) at 26°04.14N, 49°53.10E. These samples show an inverted apparent age sequence. The lowest sample (SUTL2239) from 20cm above the base bed has no measurable natural OSL signal, and appears to be modern. SUTL2237, from just below the bioturbation layer, has an OSL date of 1600±70AD. SUTL2238, which should be the youngest sample from the top of the cross bed sands 1m below the surface, has an OSL date of 1750±40AD although a significant number of discs had a larger stored dose estimate.

2/ Petrified dune (SUTL22240-2242; OSL-24, OSL-25, OSL-26) at 25°52.68N, 50°01.39E. The sample taken from the indurated sand at the top of the dune (SUTL2242) has no measurable natural OSL signal, and is modern, though a small number of disks had equivalent doses of 1±1Gy suggesting that the sample could include a small amount of older material. The sample taken from the white sand at the back of the dune (SUTL2241) has a small natural OSL signal, with low precision,

corresponding to an age of 200±150 years. The other sample taken nearby (SUTL2240) has a larger natural OSL signal with a corresponding age of 720±180 years.

3/ Barchan dune (SUTL2243, OSL-28) at 25°53.01N, 50°00.64E. This sample has a very small natural OSL signal with a corresponding age of 60±30 years. A single disk had a larger equivalent dose of 1.1±0.6Gy, suggesting that the sample could include a small amount of older material.

4/ Back of sabkha (SUTL2244, OSL-29) at 25°57.47N, 49°59.66E. This sample has a small natural OSL signal with a corresponding age of 100±50 years. Two disks had equivalent doses of 1.2±1.0Gy, suggesting that the sample could include a small amount of older material.

5/ Sabkha (SUTL2245-2246; OSL-30, OSL-31) at 25°57.33N, 50°01.33E. The sample from the top section just above the base of the white sand (SUTL2246) has a very small natural OSL signal with a corresponding age of 40±20 years. The sample from below the gypsum layer (SUTL2245) has a very large natural OSL signal with a corresponding age of 7.6±0.6ka.

6/ Old shoreline (SUTL2247, OSL-36) at 25°48.85N, 50°07.10E. The sample here has a larger natural OSL signal with a corresponding age of 5.7±0.4ka. One disk had an equivalent dose of 10.8±0.3Gy, suggesting that the sample could include a small amount of older material.

7/ Sabkha (SUTL2248-2249; OSL-37, OSL-38) at 25°46.15N, 50°09.55E. The surface sabkha sediment (SUTL2249) has no measurable natural OSL signal, and is modern. The underlying dune sands (SUTL2248) had a small natural OSL signal with a corresponding age of 160±100 years.

8/ Sabkha (SUTL2250-2253; OSL-40, OSL-41, OSL-42, OSL-43) at 25°46.69N, 50°08.08E. The top sample from sand below the sabkha sediment (SUTL2253) produced insufficient 150-250μm quartz grains for dating. Samples from the rippled sand (SUTL2253), low-angled laminated sand (SUTL2252) and slumped sand (SUTL2251) produced large natural OSL signals with ages of 1020±190 years, 940±70 years and 770±120 years respectively. It's noted that these are in an inverted order with the oldest sample higher in the section, though within 2σ the ages are the same. The lowest sample from the high-angle cross bed sand (SUTL2250) has a larger natural OSL signal with a corresponding age of 1.6±0.3ka.

9/ Sabkha (SUTL2254-2255; OSL-44, OSL-46) at 25°46.41N, 50°06.68E. The upper sabkha layer has a very small natural OSL signal with a corresponding age of 40±20years. The lower sabkha layer beneath the gypsum layer has a much larger natural OSL signal and corresponding age of 980±190 years.

10/ Sabkha sediments (SUTL2256-2257; OSL-47, OSL-48) at 25°46.09N, 50°06.45E. The sample from the upper interval (SUTL2257) has no measurable natural OSL signal, and is modern. The sample from the lower interval (SUTL2256) has a small, very low precision, natural OSL signal and a corresponding age of 100±90 years, with

one disk with an equivalent dose of 6±3Gy suggesting that the sample could include a small amount of older material.

11/ Low hill (SUTL2258-2259; OSL-49, OSL-51) at 25°58.25N, 50°00.93E.

12/ Low rolling dune (SUTL2260, OSL-53) at 25°51.86N, 50°05.59E. The sample from moderately rooted sand 50cm above the bed rock has a moderate natural OSL signal and a corresponding age of 580±55 years. Six of the discs had low precision equivalent dose measurements of 3-6Gy, suggesting that the sample could include a small amount of older material.

13/ Excavation next to new road (SUTL2261, OSL-55) at 25°48.97N, 50°03.35E. This sample has a very large natural OSL signal, corresponding to an age of 6.2±0.5ka.

14/ Small sabkha (SUTL2262, OSL-59) at 25°44.33N, 49°58.37E. This sample has a very small natural OSL signal, corresponding to an age of 50±20 years.

15/ Large sabkha (SUTL2263, OSL-61) at 25°41.10N, 49°52.54E. This sample had a large natural OSL signal, corresponding to an age of 1.25±0.15ka.

16/ Large sabkha near Hofuf river (SUTL2264, OSL-64) at 25°41.36N, 49°43.65E. This sample had no measurable natural OSL signal, and is modern.

17/ Small sabkha (SUTL2265, OSL-64) at 25°41.42N, 49°49.96E. This sample had a moderate natural OSL signal corresponding to an age of 530±50 years.

18/ Truncated top of buried dune (SUTL2266-2267; OSL-77, OSL-78) at 25°48.01N, 49°46.79E. Both the samples from this site had no measurable natural OSL signal, and are modern.

19/ Petrified dune (SUTL2268, OSL-81) at 25°53.67N, 50°02.83E. This sample had very low OSL sensitivity, and very few of the dispensed disks produced usable data. Thus, although the more sensitive disks produced a moderate natural OSL signal the age of 830±210 years has significant uncertainties.

The sabkha and shoreline samples show ages ranging from very modern (with no measurable OSL signal) to 7.6ka. In the previous work, the youngest age for a sabkha measured was 3.3±0.5ka, although some younger dates were determined for sands encroaching onto the sabkhas. The area of this study appears to have some sabkhas that are significantly younger than observed in the earlier work.

Two petrified dunes were sampled in this work. One (SUTL2268) produced a low precision OSL date of 830±210 years. The other showed very modern (with no measurable OSL signal) for the indurated sand at the top and an age of 200±150 years for the sand at the back of the dune, and an age of 720±180 years for another sample from nearby. In the previous work, relic dunes and foresets were sampled with ages from 0.5 to 13ka. One of the dated petrified dunes in this study appears to be much younger than these, with the other consistent with the youngest end of this age range.

The samples from low-rolling dunes in this study have ages between very modern and 580 years. The barchan dune sample had an age of 60±30 years, similar to ages for barchan dunes sampled in the earlier work. Samples from a low hill had ages of 2.5±0.3 and 5.7±0.5 ka. A buried dune was sampled, producing no measurable natural OSL signal.

In the earlier work (Burbidge et al 2007), dates obtained from 35 OSL measurements were related to sea-level and climatic variations in the Arabian peninsula. The data reported here can be incorporated into a similar analysis, yielding additional information about the impact of past climatic conditions on the environment of the Arabian peninsula.

References

Adamiec, G., and Aitken, M. J. (1998). Dose-rate conversion factors: update. *Ancient TL* 16, 37-49.

Aitken, M. J. (1983). Dose rate data in SI units. *PACT* 9, 69-76.

Aitken, M. J. (1985). "Thermoluminescence dating." Academic Press, London.

Alsharhan, A. S., and Kendall, C. G. S. C. (2003). Holocene coastal carbonates and evaporites of the southern Arabian Gulf and their ancient analogues. *Earth-Science Reviews* 61, 191–243.

Bøtter-Jensen, L., Bulur, E., Duller, G. A. T., and Murray, A. S. (2000). Advances in luminescence instrument systems. *Radiation Measurements* 32, 523-528.

Burbidge, C.I., Sanderson, D.C.W., and Fülöp, R. (2007). Luminescence dating of dune sand, wadi, sabkha and playa sediments, Saudi Arabia.

Burns, S. J., Matter, A., Frank, N., and Mangani, A. (1998). Speleothem based paleoclimatic record from Northern Oman. *Geology* 26, 499–502.

Davies, C. P. (2006). Holocene paleoclimates of southern Arabia from lacustrine deposits of the Dhamar highlands, Yemen. *Quaternary Research* 66, 454–464.

Ellison, S (2002). Royal Society of Chemistry AMC Technical Brief no. 6. www.rsc.org/lap/rsccom/amc/amc_index.htm

Glennie, K. W., and Singhvi, A. K. (2002). Event stratigraphy, paleoenvironment and chronology of SE Arabian deserts. *Quaternary Science Reviews* 21, 853–869.

Mejdahl, V. (1979). Thermoluminescence dating: Beta-dose attenuation in quartz grains. *Archaeometry* 21, 61-72.

Murray, A. S., and Wintle, A. G. (2000). Luminescence dating of quartz using an improved single-aliquot regenerative-dose protocol. *Radiation Measurements* 32, 57-73.

Olley, J., Caitcheon, G., and Murray, A. (1998). The distribution of apparent dose as determined by optically stimulated luminescence in small aliquots of fluvial quartz: Implications for dating young sediments. *Quaternary Science Reviews* 17, 1033-1040.

Olley, J. M., Caitcheon, G. G., and Roberts, R. G. (1999). The origin of dose distributions in fluvial sediments, and the prospect of dating single grains from fluvial deposits using optically stimulated luminescence. *Radiation Measurements* 30, 207-217.

Parker, A. G., Goudie, A. S., Stokes, S., White, K., Hodson, M. J., Manning, M., and Kennet, D. (2006). A record of Holocene climate change from lake geochemical analyses in southeastern Arabia. *Quaternary Research* 66, 465–476.

Prescott, J. R., and Hutton, J. T. (1988). Cosmic-Ray and Gamma-Ray Dosimetry For Tl and Electron-Spin- Resonance. *Nuclear Tracks and Radiation Measurements* 14, 223-227.

Prescott, J. R., and Stephan, L. G. (1982). The contribution of cosmic radiation to the environmental dose for thermoluminescent dating. Latitude, altitude and depth dependencies. *PACT* 6, 17-25.

Ratliff, L. F., Ritchie, J. T., and Cassel, D. K. (1983). Field-Measured Limits of Soil-Water Availability as Related to Laboratory-Measured Properties. *Soil Science Society of America Journal* 47, 770-775.

Sanderson, D. C. W. (1986). Luminescence Laboratory Internal Report. SURRC.

Sanderson, D. C. W. (1988). Thick Source Beta-Counting (Tsbc) - a Rapid Method for Measuring Beta-Dose-Rates. *Nuclear Tracks and Radiation Measurements* 14, 203-207.

Appendix A. Photographic record of sampling with field notes (by Steven Franks)

OSL-22 (SUTL2238). 26°04.141N, 49°53.098E. Top of cross-bedded dune sand

OSL-23 (SUTL2239). 26°04.141N, 49°53.098E. Low-angle tangential cross-bedded sand, 20cm above base bed.

OSL-25 (SUTL2241). 25°52.684N, 50°01.385E. Petrified dune. 80cm above the base at the back of the dune.

OSL-26 (SUTL2242). 25°52.684N, 50°01.385E. Petrified dune. Indurated sand from the top of the dune near the front.

OSL-28 (SUTL2243). 25°53.005N, 50°00.639E. Barchan dune

OSL-28 (SUTL2243). 25°53.005N, 50°00.639E. Shallow trench on top of the back of barchan dune.

OSL-29 (SUTL2244). 25°57.468N, 49°59.658E. Back of sabkha

OSL-29 (SUTL2244). 25°57.468N, 49°59.658E. Pit ~2m above sabkha surface

OSL-30 (SUTL2245). 25°57.328N, 50°01.333E. 76cm below sabkha surface.

OSL-31 (SUTL2246). 25°57.328N, 50°01.333E. 10cm below sabkha surface, just above base of white sand.

OSL-36 (SUTL2247). 25°48.845N, 50°07.098E. Old shoreline, trench on eastern slope.

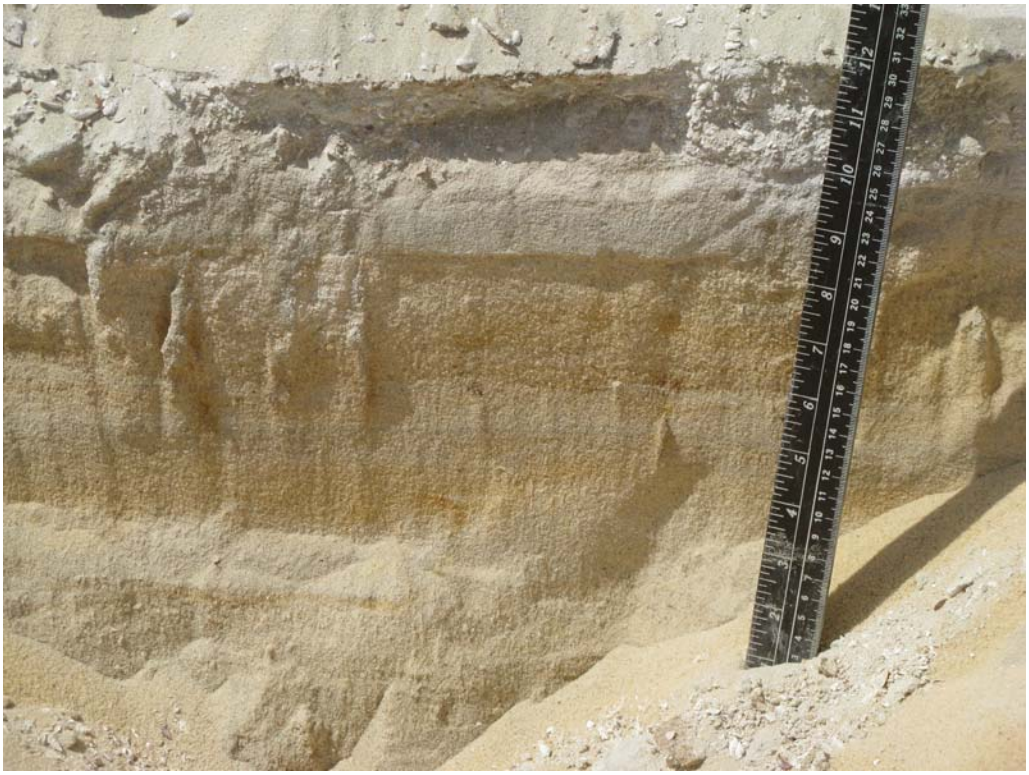

OSL-36 (SUTL2247). 25°48.845N, 50°07.098E. Crudely layered sand with thick white sand layer at top.

OSL-37 (SUTL2248) and OSL-38 (SUTL2249). 25°46.145N, 50°09.551E. Cross bedded dune sand consisting of an alternation of light and dark laminae (OSL-37), with 10cm of sabkha sediment overlay (OSL-38).

OSL-40 to OSL-43 (SUTL2250-2253). 25°46.685N, 50°08.075E. 8cm sabkha sediment overlaying 13cm ripple sand (OSL-43, top), 12cm low-angle laminated sand (OSL-42), 16cm slumped sand (OSL-41) and 40cm high-angle cross-bedded sand (OSL-40, bottom).

OSL-44 (SUTL2254) and OSL-46 (SUTL2255). 25°46.410N, 50°06.681E. 13cm of sabkha course light coloured sand overlaying 10cm of finely laminated darker sand sabkha (OSL-46, top), 9cm of gypsum sand and 44cm of sabkha sediment (OSL-44, bottom).

OSL-47 (SUTL2256) and OSL-48 (SUTL2257). 25°46.092N, 50°05.450E. Upper sabkha sediment (OSL-48) with lower, locally strong soft sediment deformation (OSL-47)

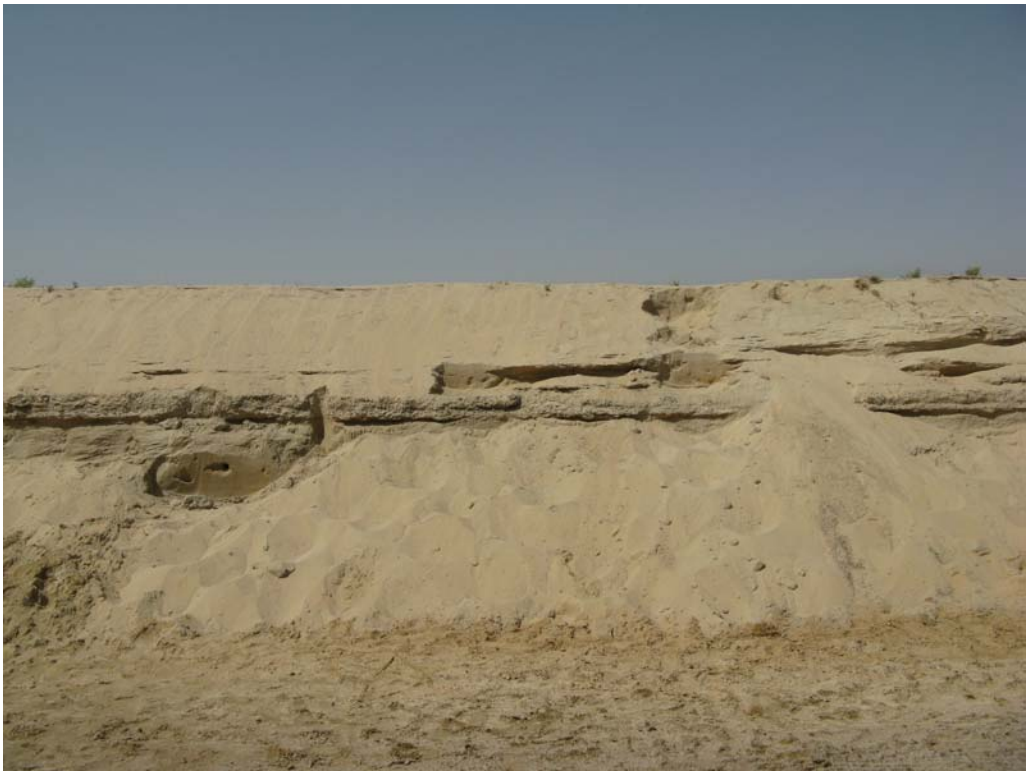

OSL-49 (SUTL2258) and OSL-51 (SUTL2259). 25°58.248N, 50°00.925E. Slope of a low hill. 76cm of crudely bedded sand (OSL-49) overlaying 27cm sand bed with small scale trough cross-bedding and 134cm of large scale cross-bedding (OSL-51).

OSL-51 (SUTL2259). 25°58.248N, 50°00.925E.

OSL-53 (SUTL2260). 25°51.863N, 50°05.586E. Low rolling dunes of circa 10m thickness developed on bed rock.

OSL-53 (SUTL2260). 25°51.863N, 50°05.586E. Sample from moderately rooted sand with subhorizontal lamination, approximately 50cm above bed rock (9.5m below dune top).

OSL-55 (SUTL2261). 25°48.967N, 50°03.353E. Horizontally laminated sand with bioturbated sand overlay.

OSL-59 (SUTL2262). 25°44.326N, 49°58.365E. Small sabkha in area of low rolling dunes. Boundary at 20cm depth separating thinner laminated sand, and thicker laminated sand below. Sample from thicker laminated sand at 40cm.

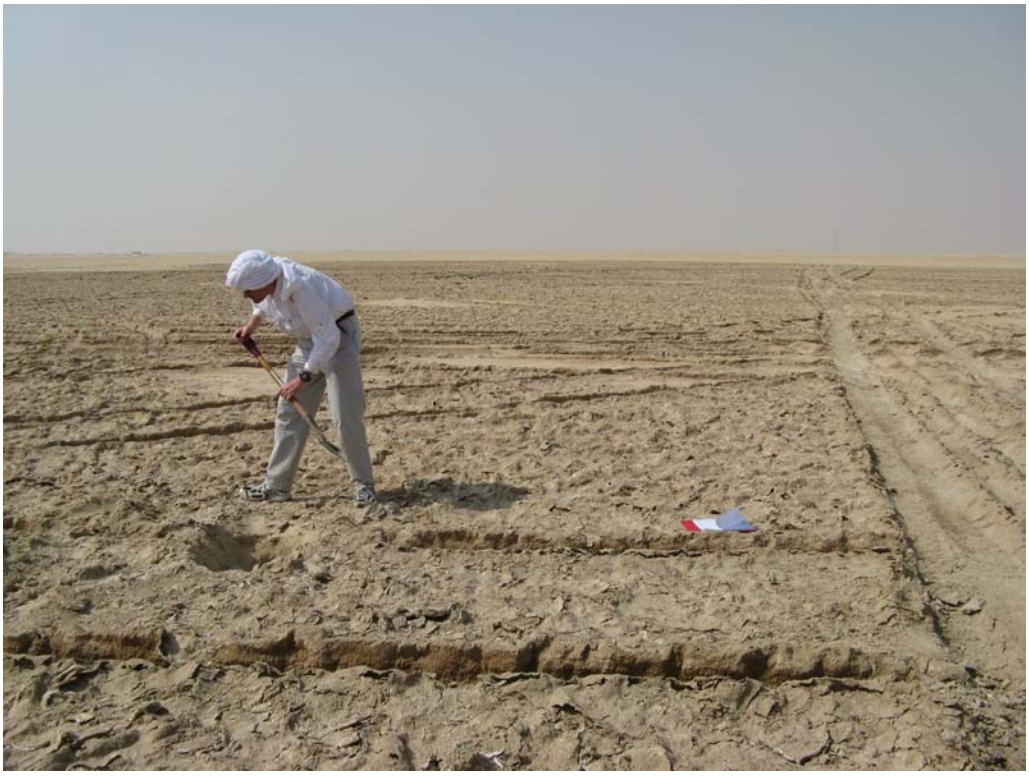

OSL-61 (SUTL2263). 25°41.104N, 49°52.537E. Large sabkha with thick halite surface crust.

OSL-61 (SUTL2263). 25°41.104N, 49°52.537E. Section shows 21cm darker sand (top), 8 cm of lighter sand, 2cm gypsum layer and 12cm indurated layer. Sample at 33cm from indurated layer.

OSL-64 (SUTL2264). 25°41.360N, 49°43.647E. Large sabkha near Hofuf river. 10cm dark sand with black lens over 15cm gypsiferous sand and 53cm of slightly wavy sand. Sample from slightly wavy sand at 53cm.

OSL-64 (SUTL2265). 25°41.419N, 49°49.964E. Small sabkha (may have been dug) in area of low rolling dunes. 7cm horizontally laminated crinkly light brown sand over 7cm sand with grey to dark and light brown colours and 26cm sand with black fill. Sample from horizontally laminated sand at 10cm depth.